



HAL
open science

Multi-scale interaction processes modulate the population response of a benthic species to global warming

Yoann Thomas, Ntsoa Rakoto Razafimahefa, Alain Ménesguen, Cédric Bacher

► **To cite this version:**

Yoann Thomas, Ntsoa Rakoto Razafimahefa, Alain Ménesguen, Cédric Bacher. Multi-scale interaction processes modulate the population response of a benthic species to global warming. *Ecological Modelling*, 2020, 436, pp.109295. 10.1016/j.ecolmodel.2020.109295 . hal-03015215

HAL Id: hal-03015215

<https://hal.science/hal-03015215>

Submitted on 23 Sep 2022

HAL is a multi-disciplinary open access archive for the deposit and dissemination of scientific research documents, whether they are published or not. The documents may come from teaching and research institutions in France or abroad, or from public or private research centers.

L'archive ouverte pluridisciplinaire **HAL**, est destinée au dépôt et à la diffusion de documents scientifiques de niveau recherche, publiés ou non, émanant des établissements d'enseignement et de recherche français ou étrangers, des laboratoires publics ou privés.



Distributed under a Creative Commons Attribution - NonCommercial 4.0 International License

1 **Multi-scale interaction processes modulate the population response of a benthic**
2 **species to global warming**

3

4 Yoann Thomas^{1*}, Ntsoa Rakoto Razafimahefa², Alain Ménesguen², Cédric Bacher²

5

6 1- Univ Brest, CNRS, IRD, Ifremer, LEMAR, F-29280 Plouzané, France

7 2- Ifremer, DYNECO, Centre Ifremer de Brest, 29280 Plouzané, France

8

9 Corresponding Author: Yoann Thomas, Institut Universitaire Européen de la Mer (IUEM),
10 Univ Brest, CNRS, IRD, Ifremer, LEMAR, F-29280 Plouzané, France; e-mail:
11 yoann.thomas@ird.fr

12

13

14

15 **Type of paper:** Original Research, Primary Research Article

16

17

18

19 **Keywords:** individual-based modelling, climate scenario, connectivity, Dynamic Energy
20 Budget, mussel, habitat, biogeography, ODD

21

22

23 1 ABSTRACT

24 Marine organisms are currently experiencing an unprecedented rate of climatic warming,
25 which affects their biogeography and threatens marine ecosystem integrity. To understand
26 how benthic species will respond to ongoing seawater warming, we assessed the relative
27 importance of processes acting at different scales using an individual-based modelling
28 approach. Our model integrates: (1) at the individual scale, interactions between the
29 environment, metabolism and ontogenic transitions; (2) at the habitat scale, competition for
30 space at settlement and mortality; and (3) at the regional scale, larval dispersal and
31 connectivity between habitats. We focused on a coastal area in the North-East Atlantic that
32 has experienced a significant seawater warming trend over recent decades. We built and ran a
33 population dynamics model for the blue mussel (*Mytilus edulis*) in this area, which is a known
34 biogeographic boundary zone. We then compared the response for a reference scenario and a
35 RCP8.5 temperature projection for 2100. We found that (1) increase in seawater temperature
36 would result in a decrease in average biomass associated with a change in recruitment
37 phenology; (2) response to seawater warming is not spatially homogeneous, showing the
38 importance of processes at the habitat scale; (3) connectivity clearly limits the consequences
39 of warming compared with other regulation processes; and (4) larval supply does not seem to
40 be a limiting factor regulating population biomass. The use of such generic models would
41 therefore be very valuable for guiding and optimizing research efforts and supporting the
42 implementation of management and conservation measures.

43 2 INTRODUCTION

44 In the domain of macroecology, process-based models are used to predict species invasion
45 rate, the effect of environmental changes on species distribution, and impact of management
46 measures on species persistence (Dormann et al., 2012). In contrast to the more popular

47 correlative models (also known as species distribution models or ecological niche
48 models), process-based models are built based on explicitly stated mechanisms, a priori
49 mathematical formulation and parameters with ecological meaning (Dormann et al., 2012).
50 Kearney (2006) even judges that only models considering the mechanistic interactions
51 between organisms and their environments can allow us to assess consequences in terms of
52 fitness and should thus be considered as ‘niche models’. With this aim in mind, Kearney et al.
53 (2010) highlighted the rationale of several theoretical mechanistic frameworks including
54 Dynamic Energy Budget (DEB) theory. DEB theory explains how organisms use energy and
55 matter throughout their life cycles. It has been widely used to simulate the life cycles of
56 benthic organisms, and some recent studies have used it to assess the consequences of climate
57 change for bivalves (Montalto et al., 2016; Thomas et al., 2016b; Thomas and Bacher, 2018,
58 Steeve et al., 2018).

59 In most studies modelling the response to environmental and climatic conditions,
60 consequences are first analysed at the individual level. However, more properties would more
61 likely emerge by upscaling from individual to population levels (Thomas and Bacher, 2018).
62 Modelling three bivalve species with temperature scenarios using DEB approach, we have
63 already shown that these different benthic species would experience significant and
64 contrasting change in population growth potential under the seawater warming conditions
65 expected in the NE Atlantic if greenhouse gas emissions continue to increase (Thomas and
66 Bacher, 2018). We also acknowledged that more realistic models should integrate processes
67 regulating population density, spatial interactions (e.g., larval dispersal and competition for
68 space) and mortality at all stages of the life cycle (e.g., ageing, starvation, predation). Such a
69 modelling framework exists and usually combines individual growth and reproduction, larval
70 dispersal through the hydrodynamic forces, mortality and competition for space, but the
71 coupling among all these processes has received only a little attention (Guizien et al., 2014,

72 2012; Le Goff et al., 2017; Ménesguen et al., 2018; North et al., 2010; Opaluch et al.,
73 2009; Puckett and Eggleston, 2016). Most often, the dispersion capacity of populations has
74 been studied as a distinct process (Coscia et al., 2013; Davies et al., 2014; Gilg et al., 2014;
75 Haase et al., 2012; Hubbard and Reidenbach, 2015; Kim et al., 2013; Lal et al., 2016; Laugen
76 et al., 2015; Nicolle et al., 2013; Thomas et al., 2016; Zhang et al., 2015). For instance, Lett et
77 al. (2010) stressed the impact of climate on the dispersal and connectivity of marine
78 populations through changes in water circulation, earlier spawning of adults, shorter durations
79 or the pelagic larval stage, reduced exposure of larvae to lethal temperatures, shorter larval
80 life and increased larval swimming speed. They called for integrated biophysical models
81 including transport, growth, behaviour, mortality and larval settlement, in an environment for
82 which both biotic and abiotic aspects are considered.

83 Since individual traits and interactions between individuals drive the dynamics of
84 populations, Individual-Based Models (IBM) are useful tools making it possible to study how
85 system-level properties emerge from the behaviour of individuals and how the system affects
86 individuals (Grimm et al., 2006). IBM represent individual organisms as entities that differ
87 from each other and change over their life cycles (Martin et al., 2012). They are characterized
88 by a set of state variables and attributes that change over time and interact with their abiotic
89 environment (e.g. habitat structure or environmental drivers such as temperature) and with
90 each other (Martin et al., 2012). The recent work by Malishev et al. (2018) illustrates how
91 combining DEB and IBM modelling frameworks allows individual behavioural strategies to
92 be compared among different habitat types.

93 In the present study, we used an individual-based population model of a marine benthic
94 species to explore how interaction processes operating at different spatial scales would likely
95 modulate the response to heat stress associated with global warming. At the individual scale,
96 the environment (i.e. temperature, food, inorganic material), individual metabolism (i.e.

97 development, growth, reproduction efficiency) and ontogenic transition (i.e. reproductive
98 phenology) interactions are formulated within Dynamic Energy Budget theory. At the local
99 scale, individuals of benthic species compete for space during their settlement phase. Larval
100 dispersal and the subsequent connectivity between habitats control the expansion of the
101 population at the regional scale of the study area.

102 Our study focuses on the blue mussel *Mytilus edulis* in a coastal area of the North-East
103 Atlantic, bordering the Western English Channel, Iroise Sea and Bay of Biscay to the south.
104 This area is known as a biogeographic boundary zone, with both boreal/cold temperate and
105 warm temperate marine faunal assemblages (Jolly et al., 2004; Southward et al., 2004). Like
106 most marine ecosystems, this area has experienced a significant seawater warming trend over
107 recent decades (Dye et al., 2013; L'Hévéder et al., 2017; Saulquin and Gohin, 2010). This
108 warming is expected to continue in coming decades, with an annual mean sea surface
109 temperature (SST) increase of 0.5°C to 2.5°C by the year 2100 depending on the
110 representative concentration pathway (RCP) scenario (L'Hévéder et al., 2017). Some
111 consequences of warming have already been identified, including warm water species
112 becoming more common (Hawkins et al., 2008; Southward et al., 2004). Projections indicate
113 that the distribution ranges of species are likely to change significantly, particularly for
114 benthic species, which are unable to escape unfavourable conditions (Fly et al., 2015;
115 Hawkins et al., 2009; Hilbish et al., 2012; Thomas and Bacher, 2018).

116 To predict the effect of temperature change with our integrated population model, we
117 compared a reference scenario with the RCP8.5 climate scenario and simulated the response
118 of populations at the regional scale of the study area. We made a detailed examination of the
119 effect of warming on model endpoints (e.g. biomass, size structure, phenology). We also
120 examined whether local density regulation (i.e. mortality, recruitment potential, competition
121 for space) and connectivity would affect the response to warming.

122

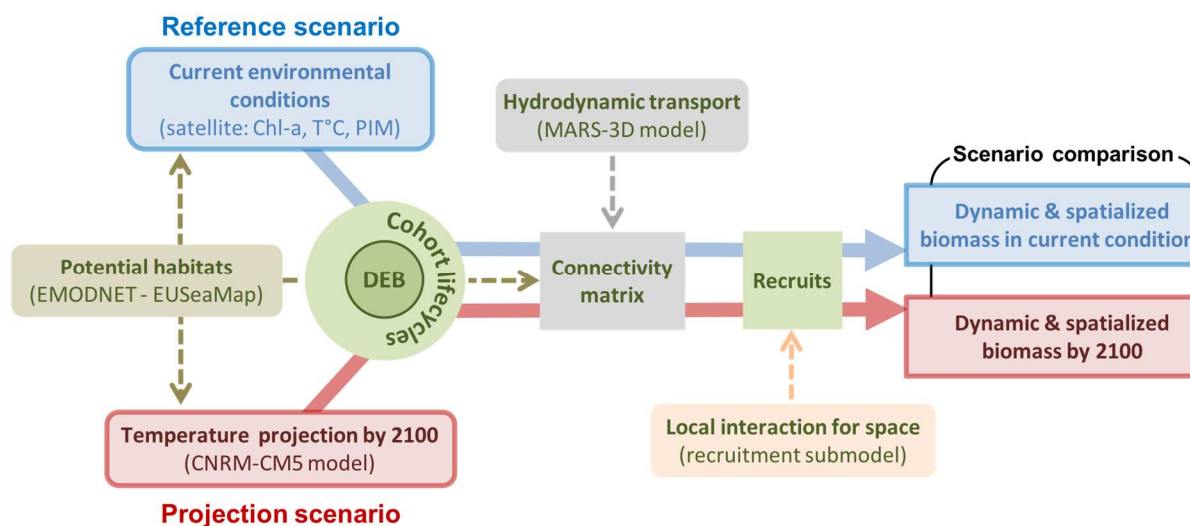
123 3 MATERIALS AND METHODS

124 3.1 Model description

125 The following sections are based on the framework of the Overview, Design concepts and
126 Details (ODD) protocol, which is a standard way to describe an individual-based model
127 (IBM) that makes writing and reading model descriptions more efficient, complete and easier
128 to replicate (Grimm et al., 2010).

129 3.1.1 Purpose of the model

130 The purpose of the present model was to evaluate how processes associated with multi-
131 scale interactions (from sub-individual to geographical scales) can modify the response of a
132 bivalve species to a climate warming scenario in rocky-shore habitats along 700 km of
133 coastline in the NE Atlantic. The model takes into account metabolic processes at the
134 individual scale through Dynamic Energy Budget (DEB) theory (Kooijman, 2010). It includes
135 a population dynamics module accounting for the spatial connectivity process between
136 habitats at the regional scale of the study area and a submodel of biotic interactions
137 (intraspecific competition for space) during the settlement phase at the local scale of habitat
138 patches (Fig. 1; details given in the following sections). The model was implemented with an
139 agent-based modelling platform: NetLogo 6.1.0 (<https://ccl.northwestern.edu/netlogo/>).



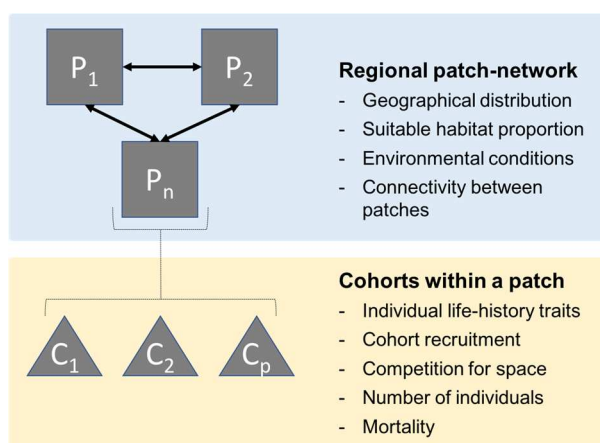
140

141 **Fig. 1. Conceptual diagram of the modelling strategy.** Reference and projection scenarios
 142 of current (blue arrow) and projected (red arrow) temperatures are compared. Biomass in
 143 potential habitats is simulated considering (1) individual metabolism with the Dynamic
 144 Energy Budget (DEB) model, (2) modelling of multiple cohorts, and (3) spatial interactions
 145 with connectivity at the regional scale of the study area and competition for space at the local
 146 scale of a habitat patch. Chl-a and PIM for the projection scenario are the same as in the
 147 reference scenario.

148 3.1.2 State variables and scales

149 We applied the model to the population dynamics of a single species, the blue mussel
 150 (*Mytilus edulis*, Linnaeus, 1758). The model simulates two entities: habitat patches and
 151 cohorts, which group individuals (Fig. 2). A regional patch network defines the geographical
 152 distribution of potential habitats in the study area. Each patch is a square space defined by its
 153 latitude, longitude, total area, proportion of suitable habitat for the species studied and
 154 environmental variables which represent the living conditions of the organisms. The model
 155 comprises a set of patches along the coasts of Brittany (France) (Fig. 3.a-b). We used the
 156 EUSeaMap broad-scale seabed habitat map to locate habitats and define the proportion of
 157 suitable habitat within each model patch, (<http://www.emodnet.eu/seabed-habitats>).
 158 EUSeaMap aims to map benthic habitats of European waters and provides access to detailed
 159 mapping of the habitats (250 m spatial resolution). Habitats are classified on the basis of
 160 seabed substrate, biological zone and hydrodynamic energy. The choice of potential habitats

161 for mussels was based on sectors belonging to the categories 'infralittoral' and 'rock and
 162 other hard substrata'. For our study, patches with potential mussel habitats were considered,
 163 from the south to the north of Brittany (Fig. 3.b). All the patches are connected, allowing the
 164 transport of larvae among patches at every spawning event (Fig. S1.b). The number of larvae
 165 transported will depend on the number of cohorts reproducing, their reproductive efficiency,
 166 and the connectivity level between the emitting and the receiving patches.



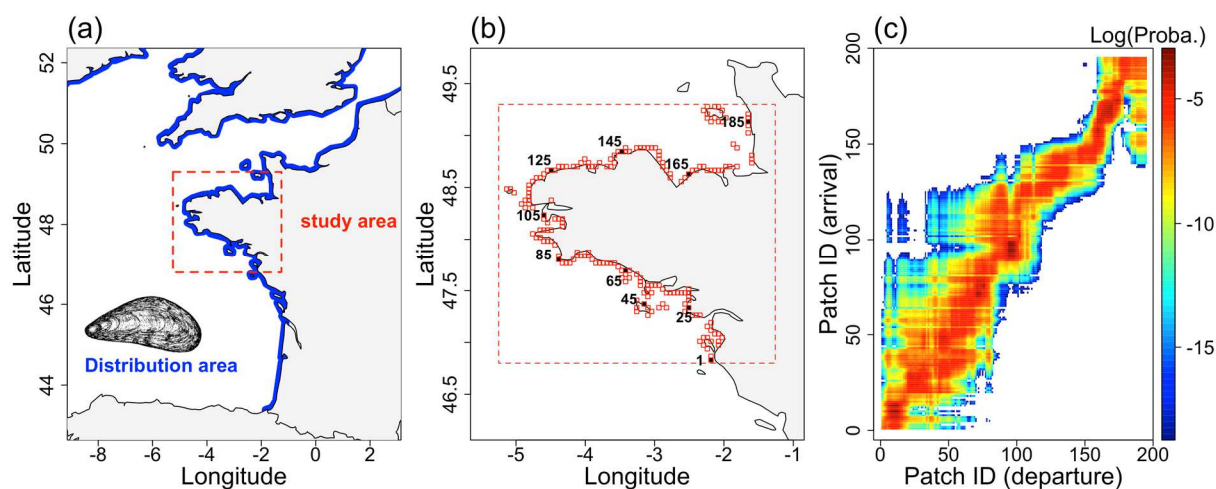
167

168 **Fig. 2. Schematic diagram of the simulated entities** in the mussel population model, indicating the
 169 relations between network, patch and cohort and the characteristics of each.

170 A cohort represents a set of individuals recruited at the same time and consequently with
 171 the same life history traits simulated by the DEB model (see section 3.1.4 'submodels'). A
 172 cohort can be thought of as a super-individual (Scheffer et al., 1995) living in a patch. Each
 173 patch can contain several cohorts and, for a given cohort, three state variables are simulated:
 174 the number of individuals, the physical length of these individuals and their reproductive state
 175 (i.e. gonado-somatic index, fecundity). Secondary variables, i.e. biomass, density, spatial
 176 coverage, recruitment, etc., are computed from these state variables at the scale of the cohort.

177 The patch, is the spatial unit of the model, a $4 \times 4 \text{ km}^2$ square corresponding to the spatial
 178 element of the hydrodynamic model MARS3D (Lazure and Dumas, 2008) used to compute
 179 connectivity in the present study (see section 3.3). The results (i.e. biomass, density) are

180 considered homogeneous at the scale of the model's patches and expressed in a reference
 181 unit of 1 m^2 . The model proceeds in discrete daily time steps.



182

183 **Fig. 3. Geographical information:** (a) map of the mussel distribution area (blue line along
 184 the coast) and location of the study area, (b) location of the potential habitats in the study
 185 area, and (c) connectivity matrix giving the connection probability between emitting (X axis)
 186 and receiving (Y axis) habitat (Log scale).

187 3.1.3 Process overview and scheduling

188 A conceptual scheme of the model's processes is given in Figure S2. At each daily time
 189 step, the individual life-history traits (growth, maturation, reproduction) of each cohort in a
 190 given patch are simulated by the DEB model and depend on environmental forcing. If the
 191 individuals are not mature, they remain in the juvenile phase and therefore continue to grow
 192 and develop but cannot reproduce. A daily mortality rate is applied to integrate all the losses
 193 occurring during juvenile and adult phases. Reproductive phenology depends on
 194 environmental conditions and may vary greatly at the regional scale of the study area. Thus,
 195 during the adult stage, spawning events are triggered when two thresholds are concurrently
 196 reached: a seawater temperature and a gameto-somatic index (GSI) threshold of 35%. GSI is
 197 defined as the mass ratio between the gametes and total dry flesh mass. Since low and high
 198 temperatures may inhibit reproduction (Fearman and Moltschaniwskyj, 2010; Lubet, 1959;
 199 Shpigel et al., 1992), lower and higher temperature thresholds inhibiting spawning were also

200 defined ($TL_{spw} = 10^{\circ}C$ and $TH_{spw} = 17^{\circ}C$). Outside of this range, individuals continue to
201 grow and to acquire energy for the development of gametes.

202 When spawning occurs within a habitat patch, the total number of larvae produced is
203 calculated based on the individual fecundity and the number of individuals releasing gametes.
204 A mortality rate is then applied to integrate all the losses occurring during the larval phase.
205 The connectivity matrix then makes it possible to evaluate the proportion of the larvae
206 produced that will be exported to other patches and the proportion that will remain in the
207 starting patch (self-recruitment). The larval phase is not explicitly simulated, spawning and
208 recruitment can occur at the same time step and new recruits all have the same initial
209 properties. However, for the purposes of modelling, individuals recruited within a given
210 temporal window are grouped into a single new cohort (see Section 3.1.4.2). Within each
211 patch receiving larvae, if enough space is available, we enter into the recruitment process. A
212 given number of recruits will settle according to the available space. Recruitment results in
213 the creation of a new cohort, with an initial number of individuals equal to the number of
214 recruits that can settle.

215 At each time step, the age and the number of individuals in each cohort, total number of
216 individuals in a habitat patch and total space occupied in each patch are simultaneously
217 updated and recorded.

218 **3.1.4 Submodels**

219 **3.1.4.1 Dynamic Energy Budget (DEB)**

220 Dynamic Energy Budget (DEB) theory offers a quantitative framework (i.e. mass and
221 energy) to model metabolic fluxes at the individual scale. These fluxes modulate substrate
222 uptake and use and sustain life-history trait dynamics: growth rate, life-stage transitions,
223 reproductive output and mortality (Kooijman, 2010). The DEB model follows the complete

224 life cycle of one individual from the embryo to juvenile and adult stages. An individual
 225 is defined by four state variables: reserves (E , unit: J), structure (V , unit: cm^3), maturity (E_H ,
 226 unit: J), and reproduction (E_R , unit: J); and seven metabolic processes (unit: $\text{J}\cdot\text{day}^{-1}$): ingestion
 227 (\dot{p}_X), assimilation (\dot{p}_A), reserve mobilization (\dot{p}_C), growth (\dot{p}_G), somatic maintenance (\dot{p}_M),
 228 maturity maintenance (\dot{p}_J), maturation and reproduction (\dot{p}_R). Life-stage successions are
 229 linked to maturity thresholds. The transition between embryo and juvenile occurs when $E_H =$
 230 E_H^b , and the transition between juvenile and adult occurs when allocation to reproduction
 231 occurs coupled with the cessation of maturation, when $E_H = E_H^p$. Somatic maintenance has
 232 priority over growth, and maturity maintenance has priority over maturation or reproduction.
 233 Details on DEB model equations and parameter values are given in the supplementary
 234 materials (Table S1 and Table S2). The individual life-history traits extracted from the DEB
 235 model were the individual physical length (L , cm), total mass (W , g) and fecundity (F , number
 236 of eggs produced). We assumed the same parameter values for males and females. DEB
 237 parameters for mussel were derived from the literature (Saraiva et al., 2012; Thomas and
 238 Bacher, 2018) (Table S2).

239 Two forcing variables, temperature and food density, modulate metabolic rates and drive
 240 individual growth and reproduction in the DEB model. When exposed to high concentrations
 241 of suspended particulate inorganic matter (PIM), bivalves maximize organic ingestion
 242 through pseudo-faeces production. We therefore introduced PIM concentration as a third
 243 forcing variable, related to the ingestion functional response ($f \in [0,1]$), following
 244 Kooijman's (2006) conceptualization:

$$245 \quad f = \frac{X}{X + K(1 + \frac{Y}{K_Y})}$$

246 where X is the food density, Y the PIM concentration, K the half saturation coefficient related
 247 to food density and K_Y the half saturation related to inorganic matter concentration. For

248 bivalve species ingestion rate, the half saturation coefficient of the functional response is
 249 known to change as a function of the food quantity and/or quality and species physiological
 250 flexibility (i.e. particle selection capacity) (Alunno-Bruscia et al., 2011). In the present study,
 251 a linear relationship between the mean Chl-a concentration and the half saturation parameter
 252 (K) was calibrated for mussel in order to take into account feeding adaptation to local
 253 conditions (see Thomas and Bacher, 2018, for calibration and validation steps performed on
 254 several datasets extracted over a wide latitudinal gradient).

255 In the DEB model, seawater temperature acts on metabolic rates following the Arrhenius
 256 function, extended over the species tolerance range, based on the idea that metabolic rates are
 257 controlled by enzymes that are inactive beyond the optimal temperature range (Kooijman,
 258 2010), and giving a temperature correction factor (T_C):

$$\begin{aligned}
 259 \quad T_C &= \exp\left\{\frac{T_A}{T_1} - \frac{T_A}{T}\right\} \\
 260 \quad &\cdot \left(1 + \exp\left\{\frac{T_{AL}}{T_1} - \frac{T_{AL}}{T_L}\right\} + \exp\left\{\frac{T_{AH}}{T_H} - \frac{T_{AH}}{T_1}\right\}\right) \\
 261 \quad &\cdot \left(1 + \exp\left\{\frac{T_{AL}}{T} - \frac{T_{AL}}{T_L}\right\} + \exp\left\{\frac{T_{AH}}{T_H} - \frac{T_{AH}}{T}\right\}\right)^{-1}
 \end{aligned}$$

262 where T is the actual temperature, T_A the Arrhenius temperature in the tolerance range, T_1 the
 263 reference temperature (20°C) for which $T_C = 1$, T_L and T_H are the lower and higher boundaries
 264 of the optimal tolerance range and T_{AL} and T_{AH} the Arrhenius temperatures beyond the lower
 265 and higher boundaries, respectively.

266 3.1.4.2 Recruitment submodel

267 At the local scale of a patch, the settlement submodel makes it possible to integrate
 268 interactions between new individuals at the time of attachment to the substrate: settlement of
 269 new recruits is only possible if there is sufficient space. If the space is limited, only a limited

270 number of individuals settle and recruit, while the others die. If there is no space, there is
 271 no settlement and all individuals die. The settlement submodel integrates the spatial
 272 connectivity, which allows the inclusion of spatial interactions between patches.

273 The recruitment submodel is based on the work of Roughgarden et al. (1985). It also
 274 incorporates the connectivity process that allows a spatially explicit approach and integration
 275 of spatial interactions between habitat patches. Recruitment therefore involves (1) evaluating
 276 the number of larvae produced, (2) integrating the connectivity process, and (3) integrating
 277 small-scale spatial interactions (intra-specific competition for space). These processes are
 278 defined in the following sections below.

279 Larval production

280 When a spawning event occurs, at time (t), the number of eggs produced in a patch i
 281 ($O_i(t)$, # number of eggs) is the cumulative number of eggs produced by the n cohorts:

$$282 \quad O_i(t) = \sum_{c=1}^n SR F_{ci} N_{ci}(t)$$

283 where SR corresponds to the population sex ratio, F_{ci} the number of eggs produced by an
 284 individual of the cohort c in patch i , and $N_{ci}(t)$ the number of individuals within the cohort c
 285 in patch i at time (t). We considered an SR of 50%, which corresponds to the mean proportion
 286 in natural populations (Yasuoka and Yusa, 2016; Yusa et al., 2013). The produced egg
 287 number is then adjusted by a mortality rate (m), including the overall mortality during the
 288 larval phase (i.e. fertilization success (FS) and daily mortality rate (M_{larvae}) associated with the
 289 pelagic larval duration (PLD)). This rate is assumed to be constant and spatially uniform. The
 290 total number of potential recruits produced in a patch i at time t ($l_i(t)$, # larvae) is:

$$291 \quad l_i(t) = O_i(t) m \text{ with } m = FS e^{-M_{larvae} PLD}$$

292 Spatial connectivity

293 The connectivity process allows the number of larvae coming from a given habitat
 294 patch to be quantified. These will then be distributed within the connected habitat patches
 295 through the larval dispersal process. The connectivity matrix synthesizes the rate of
 296 connection between every emitting habitat patch and all the others, including itself (self-
 297 recruitment). The total number of larvae received by a given patch j at time t ($L_j(t)$, # larvae)
 298 corresponds to the sum of the larvae produced in the k patches connected with j , multiplied by
 299 the connectivity rate between j and each of the k patches (C_{ij} , %):

$$300 \quad L_j(t) = \sum_{i=1}^k l_i(t) C_{ij}$$

301 where C_{ij} is the connectivity rate between patches i and j .

302 **Competition for space**

303 Occupancy of the substrata by sessile organisms can be represented by a 2-D physical area
 304 of each individual. Competition for space occurs at the time of recruitment. New recruits will
 305 only be able to settle if enough space is available to accommodate them. This available area is
 306 a function of the occupancy rate by all the individuals already recruited. It evolves over time
 307 depending on individuals' growth and mortality and the arrival of new recruits. The physical
 308 surface area occupied by an individual (b , m²) is a function of individual height (h , cm) and
 309 width (l , cm). The allometric equation for calculating the individual basal area is written:

$$310 \quad b(t) = h(t) l(t)$$

$$311 \quad \text{where } h(t) = \frac{L(t)}{\alpha} \text{ and } l(t) = \frac{L(t)}{\beta}$$

312 with allometric parameters α and β linking individual height and width to the physical length
 313 L (Alunno-Bruscia et al., 2001). This relation is needed because the DEB model only gives

314 the physical length. The cumulative surface area occupied by all individuals within a
 315 patch i (B_i , m²) is the sum of the space inhabited by all individuals of the n cohorts:

$$316 \quad B_i(t) = \sum_{c=1}^n b_{ci}(t) N_{ci}(t)$$

317 where $b_{ci}(t)$ is the individual surface coverage for cohort c in patch i at time t , and $N_{ci}(t)$ is
 318 the total number of individuals within the cohort c in patch i , at time t . The available area for
 319 recruitment in patch i ($F_i(t)$) is then obtained from:

$$320 \quad F_i(t) = A_i - B_i(t)$$

321 where A_i is the habitat area in patch i , scaled at 1 m².

322 Finally, the number of recruits will depend on the area of habitat needed by a single recruit
 323 (b_0 , m²), which then makes it possible to calculate the number of recruits per available surface
 324 unit (s , ind.m⁻²) and to calculate the number Q of recruits that can be fixed at time $(t + 1)$, per
 325 unit of space:

$$326 \quad s = \frac{1}{b_0}$$

$$327 \quad Q_i(t + 1) = sF_i(t)$$

328 Within a habitat patch, spawning events occurring at the same time step are considered
 329 together to generate a single new cohort per patch. Thus, individuals recruited within a 22-day
 330 interval, which is the mean pelagic larval duration for mussel (Sprung, 1984), are grouped
 331 into a single new cohort.

332 3.1.4.3 Changes in population abundance and biomass

333 **Mortality after settlement**

334 The number of individuals in a given cohort c and patch i at time t ($N_{ci}(t)$) is defined
 335 as follow:

$$336 \quad N_{ci}(t) = N_{ci}(0) e^{(-M a_{ci}(t))} = Q_{ci} e^{(-M(t-t_{ci}(0)))}$$

337 where Q_{ci} is the initial number of recruits for a given cohort c in patch i , M the daily mortality
 338 rate after settlement, $a_{ci}(t)$ the age of the cohort c in patch i at time t , and $t_{ci}(0)$ the time step
 339 when the cohort was created in patch i . A cohort disappears when its age ($a_c(t)$, days) reaches
 340 the lifespan of the species (a_d , days; Table S2). In the model, lifespan is assumed to be both
 341 constant and spatially homogeneous.

342 **Mussel biomass**

343 Cumulative biomass in every patch i at time (t) ($Biom_i(t)$) is computed as follows:

$$344 \quad Biom_i(t) = \sum_{c=1}^n N_{ci}(t) W_{ci}(t)$$

345 where $W_{ci}(t)$ is the individual mass for individuals in cohort c of patch i at time (t).

346 **3.2 Input data**

347 The DEB model is computed using daily time series of water surface temperature (SST),
 348 chlorophyll-a concentration (Chl-a) and particulate inorganic matter (PIM) concentration.
 349 Daily Chl-a and PIM concentration time series from 2000 to 2014 were obtained from ocean
 350 colour remote-sensing using merged SeaWiFS, MODIS and MERIS data processed using a
 351 regional algorithm specifically designed for the coastal waters of the Bay of Biscay (Gohin et
 352 al., 2002; Saulquin et al., 2011). The daily sea surface temperature (SST) was obtained from
 353 remote-sensing products from the Advanced Very High Resolution Radiometer (AVHRR)
 354 over 2000–2008 and from the Group for High Resolution Sea Surface Temperature
 355 (GHRSSST) initiative over 2009–2014 (Martin et al., 2012). Input datasets are imported in

356 NetLogo as tables, each row corresponding to one time-step and each column to a patch.
357 Time series of the individual functional response and temperatures in every patch for the
358 reference and projection scenarios are given in Figure S3a-b.

359 Following the work by Thomas and Bacher (2018), two temperature scenarios were
360 considered and compared in this study: 1) a reference (R) scenario, consisting of current
361 temperature conditions, based on the 2000–2015 period following the above description from
362 satellite information; and 2) a projection (P) scenario, consisting of predicted thermal
363 conditions at the end of the 21st century, based on the 2085–2100 period. For the latter, we
364 chose the well documented and most severe scenario, known as the ‘business as usual’
365 Representative Concentration Pathway scenario RCP8.5 (i.e. the rising radiative forcing
366 pathway leading to 8.5 W.m⁻² by 2100), which assumes that greenhouse gas emissions will
367 continue to rise throughout the remainder of the 21st century (van Vuuren et al., 2011). For
368 every location, time series of Sea Surface Temperature (SST) were extracted from the
369 CNRM-CM5 climate model outputs (from the French National Centre for Meteorological
370 Research's Coupled Model Intercomparison Project 5 (CMIP5) archive ([https://esgf-
371 node.llnl.gov](https://esgf-node.llnl.gov)), following the nearest neighbour strategy. This model demonstrated its ability
372 to correctly simulate the mean present-day SST seasonal cycle in the considered area with a
373 higher ocean resolution (1° x 1°) and more realistic topography and coastline geometry than
374 other climate models (L'Hévéder et al., 2017). SST from the climate model was available
375 with daily frequency. There is significant uncertainty in the projections of phytoplankton
376 production by climate models. Furthermore, Thomas and Bacher (2018) showed that these
377 projections would have a limited effect on population growth performance. Our projection
378 simulations therefore used the same Chl-a time series as the reference scenario. Response of
379 mussel populations along the latitudinal gradient was then studied by comparing the mean
380 biomass per unit area between the two temperature scenarios.

381 The connectivity matrix is an array with as many rows as columns, corresponding to
382 the number of patches in the model (Fig. 3.c). Each cell in the table contains a connection rate
383 between a emitting patch (column) and a receiving patch (line). The connectivity matrix was
384 derived from simulations performed by a hydrodynamic model (MARS3D) that simulates the
385 evolution of the concentrations of a tracer emitted in each potential habitat mesh square and
386 dispersed over a period of 22 days. The emitted particles were considered to be passive, with
387 no vertical migration behaviour considered. The mesh size of the hydrodynamic model is 4 x
388 4 km. Computing the connectivity matrix for several decades was not possible. Connectivity
389 simulations were thus performed monthly for a given year to represent the mean conditions
390 encountered over a long period and maintain realistic forcing. The year 2005 was chosen after
391 an analysis of wind conditions over 10 years, which showed that this year was the closest to
392 the climatology of this area.

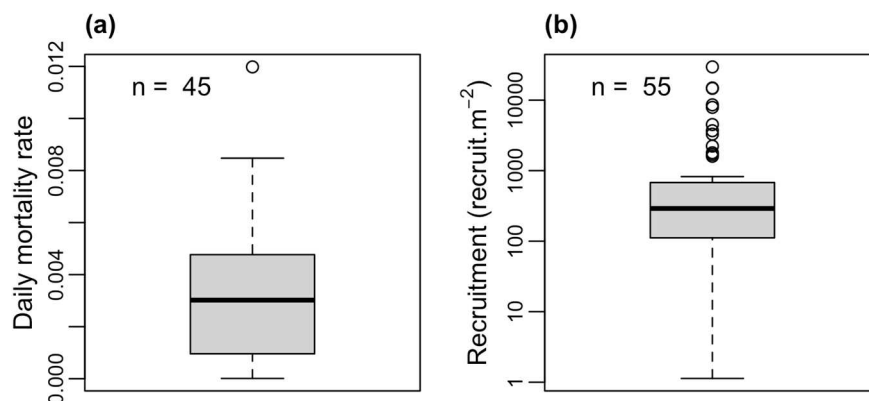
393 **3.3 Initialization**

394 At the initial time step, one single cohort with 50 ind.m⁻² is created in every patch. All
395 individuals are similar and considered to be at the post-metamorphosis stage. Time series of
396 simulated biomass in every patch are given in Figure S3c for the reference and projection
397 scenarios, with identification of the spin-up and analysed periods. A spin-up time of three
398 years is long enough for the emergence of a stable pattern of abundance and biomass at the
399 scale of the study area and was applied before analysing the model results over a period of 15
400 years.

401 **3.4 Model calibration and performance evaluation**

402 A set of data was extracted from the literature (Table S3) for the calibration of two
403 parameters: the post-settlement mortality rate (M) and the number of recruits per available
404 surface unit (s) (Fig. 4). The median was chosen because of the asymmetrical dispersion of

405 the data. Model performances were then evaluated with these values, with regard to the
 406 simulated mussel density, space coverage, number of recruits 10 months post-settlement and
 407 mussel size distribution. Due to the uncertainty associated with these density control
 408 parameters, we performed a sensitivity analysis on them (see next section).



409

410 **Fig. 4. Observed (a) mortality rate and (b) recruitment density** used for the model
 411 calibration step. Medians were used for model parameterization: $M = 0.003 \text{ d}^{-1}$; $s = 290$
 412 recruits.m^{-2} .

413 3.5 Sensitivity analysis

414 A first step, in order to evaluate stability and potential edge effects, was to assess the effect
 415 of the spatial model fit on the results. Three zoom levels were compared, corresponding to
 416 three spatial coverages, with differences between biomass variations related to temperature
 417 scenario computed between each pair of zooms. A description of these preliminary results is
 418 given in the supplementary material (Fig. S4, Fig. S5 and associated text), and led us to
 419 choose one zoom level as the study area for the subsequent analyses.

420 A set of sensitivity analyses was then conducted to assess the effect of interaction
 421 processes occurring at different spatial scales on the response to the temperature scenarios.
 422 We tested the effect of the connectivity, which represents interactions occurring at the
 423 regional scale of the study area and the effect of larval and adult mortality and recruitment
 424 potential, which are related to processes occurring at the local scale of habitat patches.

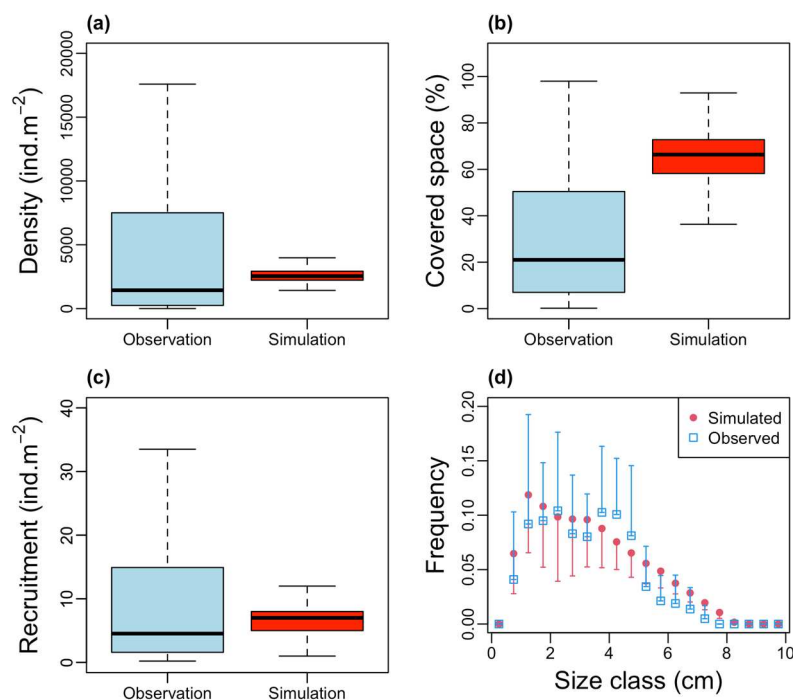
425 For the connectivity scenarios, the results obtained with a reference connectivity
426 scenario (i.e. monthly connectivity, PLD = 22 days) were compared with a scenario without
427 connectivity, under which there was only self-recruitment, considered to be average and
428 uniform over the whole area, corresponding to the average value of the connectivity matrix
429 diagonal. Since temperature has the effect of shortening the duration of the pelagic larval
430 phase, we tested a connectivity scenario with a PLD of 19 days, which reduced the dispersal
431 potential and larval mortality. Finally, in order to assess the impact of seasonal variability in
432 connectivity patterns associated with the reproductive phenology (i.e. seasonality of the
433 spawning events), we compared the baseline scenario with year-averaged connectivity
434 scenarios in each habitat for each PLD (i.e. 19 and 22 days).

435 For the sensitivity analysis of mortality and recruitment potential, we applied factors of \pm
436 10% and \pm 50% to the mean values of larval mortality (m), adult daily mortality rate (M) and
437 number of recruits per unit area (s). We ran simulations for both temperature scenarios and
438 compared the responses to temperature changes obtained with the modified parameter values
439 with the results obtained with the mean values.

440 In every patch and at each time step, simulated values were output and stored in the form
441 of .CSV files for (1) individual life history traits (size, weight, gonado-somatic index,
442 spawning efficiency) for each cohort, (2) population structure (density per cohort,
443 recruitment), and (3) habitat cover rates in all patches. All these outputs were used to perform
444 post-treatment with R software (R Development Core Team, 2012).

445 **4 RESULTS**446 **4.1 Model performance evaluation**

447 Our simulated mean densities, coverage rates and recruitment observed 10 months after
 448 fixation (Fig. 5.a-b-c) are not significantly different from the observations (t-test, $p < 0.05$).
 449 The simulated mean size distribution at the patch scale matches the mean size distribution
 450 produced by a set of observations (Fig. 5.d). The variance measured in the observations is
 451 well reproduced by the simulated monthly profiles, which show the evolution of mussel sizes
 452 distribution over the year as a result of recruitment, growth and mortality processes.
 453 Simulated maximum lengths around 8 cm are consistent with observed data, although the 4
 454 cm class appears underestimated and the 6 cm class overestimated by the model.

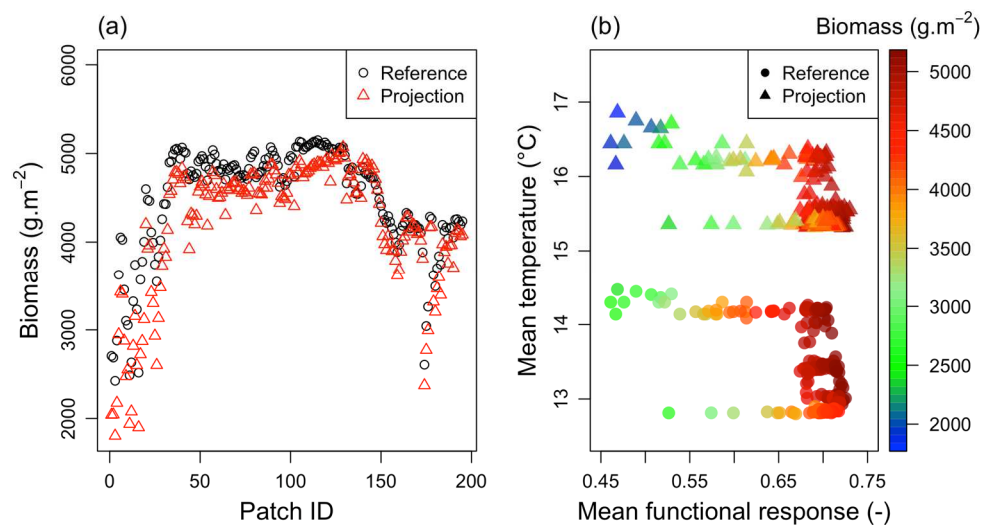


455

456 **Fig. 5. Comparisons of the IBM predictions with data from the literature.** (a) Observed density ($n = 71$), (b) covered area ($n = 37$) and (c) recruitment density after 10 months ($n = 53$). No significant
 457 differences were found between observations and simulations (Student test, $p < 0.05$). (d) Individual
 458 size (i.e. length) distributions: observations refer to a set of published data (mean \pm STD; see Table
 459 S3) and simulations to the monthly average distributions for all patches, error bars represent the
 460 monthly variability (i.e. STD; half of error bars are drawn for readability).
 461

462 4.2 Effects of seawater warming conditions

463 Under reference temperature conditions, simulated biomasses differ along the latitudinal
 464 gradient (Fig. 6.a). Lower biomasses are simulated in southern areas and range from 2425
 465 $\text{g}\cdot\text{m}^{-2}$ to more than 5150 $\text{g}\cdot\text{m}^{-2}$ close to patch 110. In the projection scenario, the geographical
 466 pattern of simulated biomass remains identical to that of the reference scenario, with a
 467 decrease in absolute values south of patch 125: min/max = 1805/5070 $\text{g}\cdot\text{m}^{-2}$. Biomasses
 468 plotted in temperature-food space can be viewed as the realized population niche (Fig. 6.b).
 469 Large differences were simulated along the food gradient, with a positive and significant
 470 relationship (linear regression: $R^2 = 0.73$; $p < 0.001$), accounting for over 110% of variation.
 471 Response across the thermal range appears lower, with variations related to warming reaching
 472 -27%.

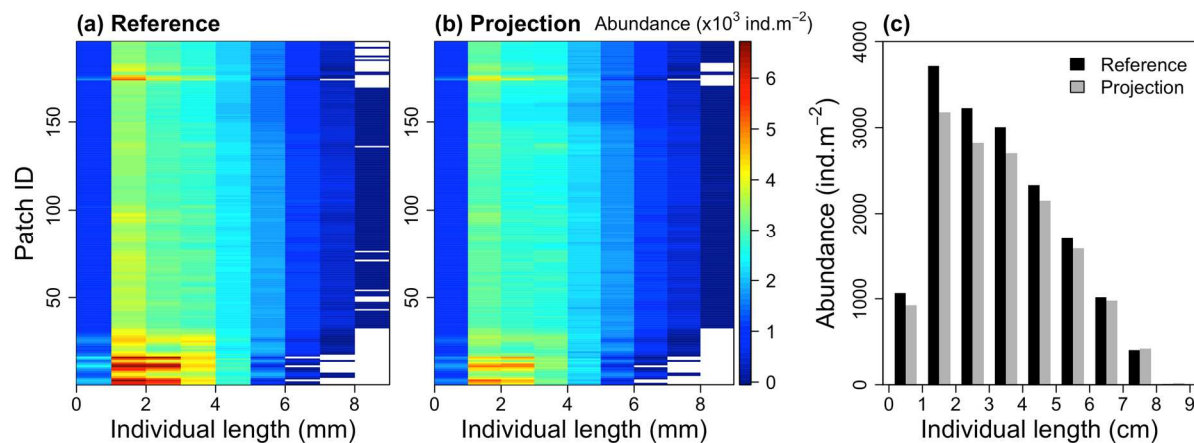


473

474 **Fig. 6. Simulated biomass in reference and projection scenarios:** (a) mean biomass simulated in
 475 every patch (patches are ordered from south to north of the study area) and (b) mean biomass
 476 simulated in every patch as a function of mean temperature and individual functional response (i.e.,
 477 food effect) for the two temperature scenarios.

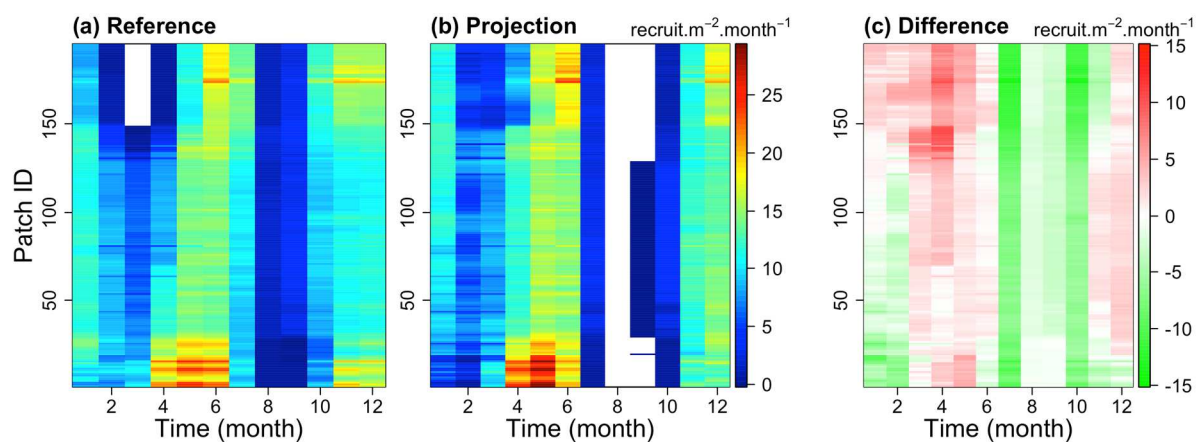
478 The mussel size distribution is modified by the seawater warming projection scenario (Fig.
 479 7). Abundance of small individuals is significantly lower throughout the study area. This
 480 difference results in a mean individual length of 3.37 cm in the projection scenario compared
 481 with 3.29 cm in the reference scenario. This change in size structure is accompanied by a

482 clear change in reproductive phenology (Fig. 8). A total halt in recruitment is simulated
 483 during the summer period throughout the study area. This phenomenon is associated with the
 484 upper temperature threshold applied for reproduction. Conversely, the effect of the lower
 485 threshold seems to be noticeable in the northern part of the study area (patch > 125), with an
 486 activation of recruitment during winter, which is not observed in the reference scenario. The
 487 overall average recruitment rate is thus significantly reduced from 9.3 to 8.2 recruits.m⁻².
 488 month⁻¹ between the reference and projection scenarios, respectively. The patches in the
 489 south of the study area appear to be the most heavily penalized by decreased recruitment.



490
 491 **Fig. 7. Size frequency simulated over the studied area in the reference and projection scenarios:**
 492 (a) monthly mean size frequency (expressed as abundance) in every patch in the reference scenario,
 493 (b) monthly mean size frequency (expressed as abundance) in every patch in the projection scenario
 494 and (c) monthly mean abundance, averaged over the studied area for the two scenarios.

495



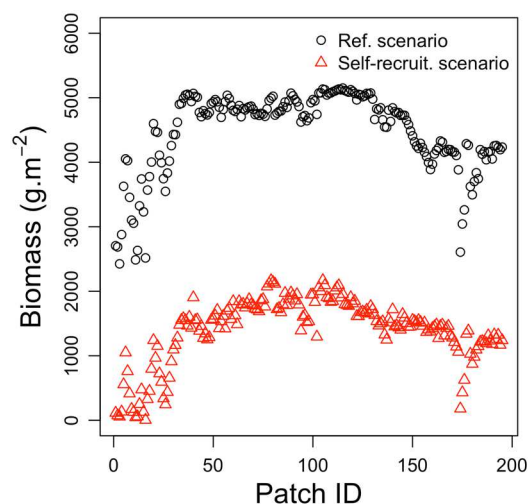
496
 497 **Fig. 8. Seasonal recruitment simulated over the studied area in the reference and projection**
 498 **scenarios:** (a) monthly mean number of recruits in every patch in the reference scenario, (b) monthly

499 mean number of recruits in every patch in the projection scenario and (c) difference in mean
 500 number of recruits between the two scenarios (projection - reference) in every patch.

501 4.3 Sensitivity analysis

502 4.3.1 Connectivity effect

503 As previously described, simulated biomasses with the reference scenario (i.e. current
 504 temperature, monthly connectivity, PLD = 22 days, average mortality and recruitment
 505 potential) show geographical heterogeneity, with lower biomasses in the south of the study
 506 area (Fig. 9). Biomasses stabilize in the centre of the study area (patch ID > 40), before
 507 decreasing again in the north of the area (patch ID > 150). When connectivity between
 508 patches is removed and only self-recruitment is considered, this general pattern of biomass
 509 variation is maintained, but biomasses are significantly lower. Average biomass decreases
 510 from 4480 ± 620 to 1401 ± 510 g.m^{-2} , corresponding to a mean decline of 69%. Habitats in
 511 the south of the area can show biomasses very close to 0 g.m^{-2} (min = 5 g.m^{-2}).

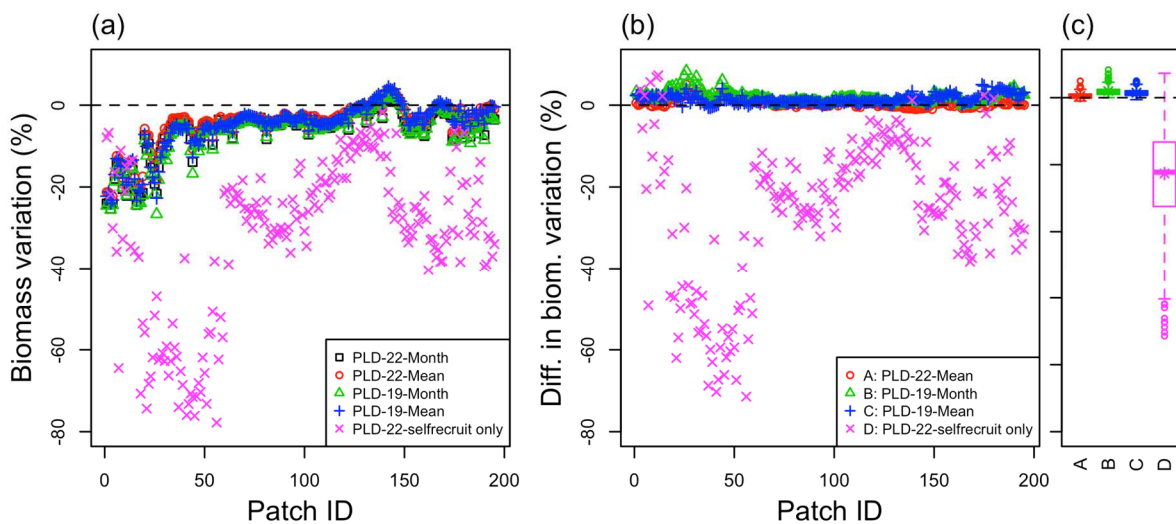


512

513 **Fig. 9. Effect of population connectivity on simulated mussel biomass:** biomass simulated in every
 514 habitat for the reference temperature scenario and with connectivity (ref.) or self-recruitment only.
 515 Data are averaged over the simulated period (15 years).

516 Beyond the direct effect on biomass, the simulations highlight that connectivity also
 517 mitigates the effect of the seawater warming scenario. If connectivity is removed and there is

518 only self-recruitment, the decrease in biomass in the projection scenario is enhanced. On
 519 average, there is 22% lower biomass compared with the baseline simulation with monthly
 520 connectivity (Fig. 10.b-c). The other connectivity scenarios show that there is a limited effect
 521 of PLD and seasonal variation on biomass patterns. The three scenarios associated with PLD
 522 equal to 19 days and year-averaged connectivity tend to slightly limit the effect of warming
 523 by limiting biomass decline. Simulations show that the response has a spatial structure, with
 524 higher sensitivity in the south (patches 20 to 60) (Fig. 10.b). A possible edge effect appears at
 525 the extreme southern end of the study area, with results converging between the scenarios
 526 with and without connectivity.



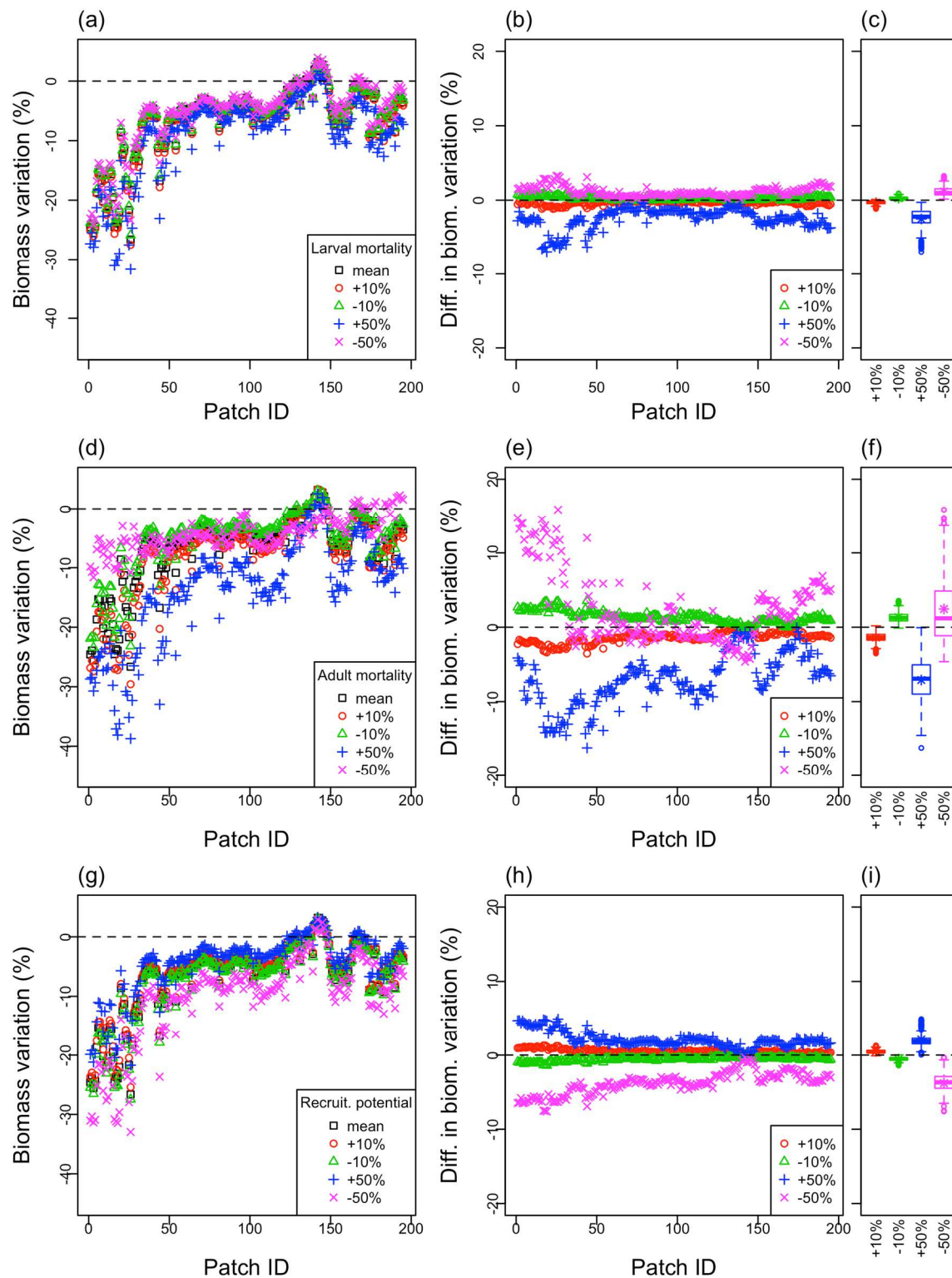
527

528 **Fig. 10. Effect of habitat connectivity on mussel response to seawater warming scenario**
 529 **(RCP8.5):** (a) difference in simulated biomass between the reference (R) and projection (P)
 530 temperature scenarios ($100 \times (P - R) / R$, %) in each patch and for each connectivity scenario, (b)
 531 difference in biomass variation between the realistic connectivity scenario ('PLD-22-Month') and the
 532 others, and (c) boxplot of the differences results, summarizing panel (b) for each connectivity
 533 scenario.

534 4.3.2 Mortality and recruitment effects

535 Whatever the scenario regarding mortality or recruitment potential, the response to the
 536 projection scenario shows the same pattern, with a decrease in simulated biomass in most of
 537 the habitats studied (Fig. 11.a, d, g). In a similar way to the reference model (monthly
 538 connectivity; PLD = 22 days; mean mortality and recruitment potential), the decrease in

539 biomass is greater in the south of the study area. The effect of the mortality and
540 recruitment potential scenarios on response to warming is relatively limited and differences
541 with the reference model do not exceed 6% on average. However, this modulation is spatially
542 heterogeneous. Southern habitats are systematically more sensitive and show larger
543 differences from the reference model. The modulation is also non-symmetrical depending on
544 whether the factor under consideration is increased or decreased. Increases in larval or post-
545 larval mortality and decreases in recruitment potential have a greater effect on response to
546 warming than decreases in these parameters.



547

548 **Fig. 11. Response to seawater warming scenario as a function of (a-c) larval mortality, (d-f)**
 549 **adult mortality and (g-i) recruitment potential.** For each process tested, the three panels correspond
 550 to: (a, d, g) change (%) in simulated biomass between the reference (R) and projection (P) temperature
 551 scenarios ($100 \times (P - R) / R$), in each patch; (b, e, h) difference in biomass variation between the
 552 realistic scenario (here 'Mean') and the others; and (c, f, i) boxplots of the differences results,
 553 summarizing the second panel for each scenario.

554 **5 DISCUSSION**

555 **5.1 Results highlights**

556 Our results confirm the poleward latitudinal shift of a species distribution range resulting
557 from global warming (Jones and Cheung, 2015; Jones et al., 2010). With the RCP8.5
558 scenario, our simulation showed a decrease in biomass ranging from -27% in the south to 0%
559 in the north of the study area, under the most realistic modelling conditions. We found that
560 this decrease is related to a change in recruitment success and shift in reproduction
561 phenology. This confirms previous results on the importance of reproductive phenology in the
562 response of bivalve species to seawater warming (Thomas et al., 2016; Thomas and Bacher,
563 2018). The consequences of such an evolution are numerous for fishery and aquaculture
564 activities (e.g. reduction in individual growth, standing stock biomass and recruitment
565 success), but also for the balance of ecosystems (e.g. benthic-pelagic coupling, biodiversity
566 associated with reef building, food web equilibrium). Our modelling approach is generic and
567 is therefore applicable to many species with a benthic-pelagic life cycle. This would make it
568 possible to evaluate consequences at the ecosystem scale, particularly by assessing the effects
569 on material flows (biomasses, filtration rates, biodeposition, etc.) and food webs (impact on
570 biodiversity at the local scale).

571 Previous studies did not account for the process of connectivity between populations or
572 density regulation processes at the local scale of mussel patches (i.e. competition for space),
573 which allow a realistic representation of biomass dynamics. In the present work, we modelled
574 these processes of regulation and spatialization, allowing a relevant representation of
575 population densities and size structures, comparable to data available in the literature. Our
576 results highlight four major findings: (1) the temperatures projected by the RCP8.5 climate
577 scenario to 2100 imply a decrease in average biomass and a shift in reproductive phenology,

578 (2) the modulation response to temperature change is not spatially homogeneous,
579 showing the importance of the processes implemented at the local scale, (3) the connectivity
580 process clearly limits the consequences of seawater warming compared to other regulation
581 processes, and (4) the larval supply does not seem to be a limiting element and only slightly
582 modulates the response to temperature change. We will next examine the assumptions and
583 implications of our results.

584 **5.2 Importance of local-scale processes: habitat definition**

585 The ecological niche concept locates species in the optimal zone of the environmental
586 space that regulates their biomass. By considering temperature and food (here modulated by
587 the density of inorganic particles), we have shown that the heterogeneity of trophic conditions
588 is a key element that explains a large part of the simulated biomass variability. Nearly 110%
589 biomass variation was simulated between the most contrasting habitats in our baseline
590 scenario along the trophic gradient, compared with a maximum of -27% along the thermal
591 gradient. However, our approach does not consider the complexity of the thermal conditions
592 that may exist at a small scale. This has already been well demonstrated in rocky intertidal
593 habitats, notably through the concept of a mosaic of thermal environments (Helmuth et al.,
594 2002). Since our study area was not located at the extreme limit of the species range, we
595 considered that the temperatures used should reflect average conditions and that the
596 physiological extremes were not reached. However, this assumption highlights the importance
597 of considering the processes prevailing at a small scale that modulate both physiological
598 performances and biotic interactions.

599 Here, we defined the potential habitat as rocky intertidal areas, which were derived from
600 the products of the European EMODNET Seabed Habitats project (Thomas and Bacher,
601 2018). In our model, we hypothesized that colonization of this habitat by mussels would take

602 place depending on two conditions: i) local food concentration must support mussel
603 individual growth and reproduction, and ii) connectivity between habitats and self-recruitment
604 within a given habitat would maintain the recruitment of individuals high enough to
605 compensate for the mortality of new recruits, juveniles and adult mussels. All our modelled
606 patches match these conditions. We also accounted for the competition for space using a
607 simple rule linking space availability to the size and density of mussels already present in a
608 patch. Simulations showed that all the space was eventually occupied, and we found that
609 differences between patches and temporal variability of mussel density merely resulted from
610 growth differences due to local food concentration. Therefore, the predicted mussel density
611 and biomass can be seen as proxies of the actual values, and the results interpreted in terms of
612 the relative differences between scenarios.

613 More realistic predictions of mussel biomass would require i) a better estimation of the
614 area of potential habitat within each patch and ii) to determine the local factors that limit the
615 occupation of potential habitat (i.e. realized habitat). The spatial resolution of the EMODNET
616 layers we used to identify the different type of habitats may be not sufficient to represent
617 coastal intertidal habitats, though we do not know of any work addressing this issue. Spatial
618 resolution is an issue addressed in Species Distribution Modelling, and some authors have
619 shown that it has an effect on model performance (Lowen et al., 2016). Gomes et al. (2018)
620 recently presented the advantages of aerial photography for investigating large-scale patterns
621 of mussel distribution in intertidal mud and sand flats. They pointed out the lack of studies
622 quantifying mussel distribution on rocky shores and demonstrated how the use of aerial
623 photography with a drone helps us to understand mussel distribution in such habitats.
624 Through the combination of image analysis and habitat suitability model at a high spatial
625 resolution, they mapped the density, mean size and reproductive effort of *Mytilus*
626 *galloprovincialis* along the Portuguese rocky intertidal coastline. Density ranged from 0 to

627 6500 ind.m⁻², which compares well with the values we found with our model. Mussel
628 coverage (ratio mussels/rocky substrate) varied between 0.4 % up to 60% depending on
629 location. They also found a significant relationship between wave exposure and the density
630 and distribution of mussel populations and argued that wave action forces intertidal organisms
631 to adapt and withstand the dynamics of water motion. Physical drivers would explain, at least
632 partly, the distribution of mussel populations, and Gomes et al. (2018) concluded that
633 location-specific predictions can be used in metapopulation models. Considering the effect of
634 physical drivers in addition to the bioenergetics of organisms and the connectivity between
635 patches would, therefore improve the quantitative predictions of our models. The
636 development of habitat observation tools (e.g. high-resolution photogrammetry) combined
637 with tools for modelling (e.g. microclimate conditions, Kearney et al., 2020) offer promising
638 prospects in this context (Choi et al., 2019).

639 **5.3 The two sides to larval supply: larval production and connectivity**

640 'Supply-side ecology' recognizes that variable larval input is a key factor determining the
641 size of local adult populations (Hughes et al., 2000). However, as Hughes et al. (2000) point
642 out, the spatial scale at which adult stocks and recruitment are coupled is unknown for most
643 marine organisms. By decoupling these two processes, our results highlight the lower effect
644 of larval supply relative to the connectivity potential. A variation of $\pm 50\%$ in larval mortality,
645 which could be associated with a significant decrease in reproductive efficiency, modulates
646 the response to the projection scenario by less than $\pm 5\%$, compared with the -22% simulated
647 by our 'self-recruitment' scenario. The comparison between the 'self-recruitment' and
648 reference (with connectivity) scenarios also showed that the response of mussel biomass to
649 temperature change was more sensitive to connectivity than to any other factor we tested (Fig.

650 S6). Mussel biomass would also be reduced by 70% if self-recruitment was the only
651 process of population renewal.

652 Our simulations also give an idea of the dispersal capacity and dispersion range of mussel
653 populations. Additional simulations (Fig. S7) indicate that the southernmost mussel
654 population in this study would need 13 years to reach the most northern set of patches and
655 that mussels never propagate from north to south, reflecting the asymmetry in the
656 connectivity matrix and breakpoints associated with environmental conditions limiting
657 sufficient reproductive capacity. Ayata et al. (2010) simulated connectivity in the same region
658 and also showed that the Ushant Sea, which lies between the western English Channel and
659 northeast Bay of Biscay, likely acts as a partly permeable one-way barrier. However, there is
660 very little quantitative information on spatial dispersion of mussel propagules, and most
661 observations, calculations or hypotheses give values between a few kilometres up to 100 km.
662 In their modelling of mussel dispersion along the French Atlantic coast, Wetthey et al. (2011)
663 assumed that the spatial scale of dispersal was 25 km and argued that this value is typical of
664 the dispersal ranges of intertidal species with planktonic larvae. In South Africa, McQuaid
665 and Phillips (2000) found that the dispersal radius would maintain 90% of the intertidal
666 mussel *Mytilus galloprovincialis* population within an area of 5 km, while the maximum
667 effective dispersal of mussel larvae in this area would be less than 100 km. Gilg et al. (2007)
668 found exchanges of *M. edulis* and *M. galloprovincialis* larvae possible over distances >100
669 km though barriers to dispersal could occur at some locations. For another mussel species,
670 model projections made by Gilg et al. (2014) suggested that dispersal distance could exceed
671 100 km. Carsons et al. (2010) identified larval source populations of mussels species and
672 found dispersal distances around 35 km. These examples show that, for intertidal species like
673 mussels, hydrodynamics control the spread of populations and should be investigated in more
674 detail. Following the work of Nicolle et al. (2017) and Ménesguen et al. (2018) on other

675 benthic species, it would be interesting to extend our calculation to a larger set of
676 patches extending to the north of the English Channel and to assess the kernel and barriers to
677 dispersion at a larger spatial scale.

678 **5.4 Larval behaviour and phase duration**

679 We assumed that the pelagic phase duration was spatially homogeneous and constant in a
680 given scenario, and that the larvae were transported passively, with no swimming behaviour.
681 Testing the effect of pelagic larval phase duration showed that changes of biomass in response
682 to temperature change were not very sensitive to this parameter.

683 We have not found any similar studies addressing the effect of larval swimming on mussel
684 larvae dispersion and metapopulation connectivity. Other authors made different assumptions
685 depending on the species of interest, modelling scope or available information, and
686 conclusions on the need for incorporating behaviour do not converge. McQuaid and Philipps
687 (2000) estimated that passive transport was sufficient to explain the abundances of larvae in
688 their region of interest. Kim et al. (2013) found that physical forcing showed a greater
689 influence on the loss of *C. virginica* larvae than did behaviour. but North et al. (2008) found
690 that behaviour had significant consequences for dispersal distances, transport success, and the
691 degree of connectivity between subpopulations. Hubbard and Reidenbach (2015) follow the
692 same line, concluding that changes in swimming behaviour due to turbulence influence the
693 probability of settling of *C. virginica* on suitable substrate. This apparent contradiction
694 regarding the need, or lack thereof, to account for larval behaviour, can be explained by
695 sources of variability considered and the hypotheses tested. In our model, we emphasized
696 multiple spawnings within mussel populations, due to local differences in individual growth
697 and reproduction. Emissions of larvae at different times of the year would generate new
698 cohorts of individuals with different life histories and spawning events. This cascade effect

699 yields a large variability of life history traits within each population and contributes to
700 the variability of larval transport.

701 **5.5 Conclusion**

702 The effect of a climate warming scenario, currently considered to be the most severe of the
703 projections, appears to be strongly modulated by processes occurring at multiple scales. At
704 the local scale, food availability remains a major factor structuring biomass, and neither
705 ontogenic mortality nor recruitment potential seem to strongly modulate the response. At the
706 study area scale, the connectivity between populations mitigates the consequences of warming
707 by limiting the loss of biomass locally. These results are made in a restricted biogeographic
708 transition zone. The same approach would merit being established over the entire range of the
709 species to assess whether this observation remains homogeneous. The generic nature of the
710 approach developed will also make it possible to compare the response of other species.

711 Our model is constructed of solid elements, based on well-established theories and
712 processes. It produces results that have demonstrated their realism and robustness to
713 sensitivity analysis. We need, however, to know more about the realized habitat in order to
714 have a more quantitative approach of realized niche. Connectivity appears to be a determining
715 factor, and patterns of population connectivity could be strongly modified by local processes
716 limiting the occupation of potential habitats. The next step in the implementation of such a
717 population dynamics modelling approach would be to have a more realistic representation of
718 the realized habitat, in order to get as close as possible to the true connectivity (*sensu* Watson
719 et al., 2010).

720 Identifying and prioritizing the processes likely to modulate the multi-scale response of
721 species to climate change is a key element in predicting the dynamics of marine ecosystems in
722 a context of increasing pressures such as seawater warming, hypoxia events, acidification,

723 overexploitation, pollution, etc. As biological responses, socio-economic and
724 administrative aspects are not spatially homogeneous (Barillé et al., 2020), the integration of
725 spatial processes into a spatially explicit modelling (SEM) strategy appears to be the decisive
726 difference from spatially implicit models (SIMs), which are more oriented towards theoretical
727 issues (DeAngelis and Yurek, 2017). The use of such models, with a generic approach, would
728 make it possible to provide scientific support to guide and optimize research efforts, e.g.
729 define key field observations, experimentation and operational modelling strategies, and
730 support the implementation of management and conservation measures.

731 **6 ACKNOWLEDGEMENTS**

732 This research was supported by a grant from Région Bretagne (SAD POPDEB n°9277)
733 and Ifremer. Authors thank M. Vasquez (Ifremer, DYNECO) for assembling the EUSeaMap
734 seabed habitat mapping information and C. Cassou (CNRS, Cerfacs) for putting together the
735 climate model datasets. We thank Helen McCombie for English editing and her valuable
736 comments and anonymous reviewers for their comments which improved our manuscript.

737 **7 REFERENCES**

- 738 Alunno-Bruscia, M., Bourget, E., Fréchette, M., 2001. Shell allometry and length-mass-
739 density relationship for *Mytilus edulis* in an experimental food-regulated situation.
740 *Marine Ecology Progress Series* 219, 177–188.
- 741 Alunno-Bruscia, M., Bourlès, Y., Maurer, D., Robert, S., Mazurié, J., Gangnery, A.,
742 Gouletquer, P., Pouvreau, S., 2011. A single bio-energetics growth and reproduction
743 model for the oyster *Crassostrea gigas* in six Atlantic ecosystems. *Journal of Sea*
744 *Research* 66, 340–348.
- 745 Ayata, S.-D., Lazure, P., Thiébaud, E., 2010. How does the connectivity between populations
746 mediate range limits of marine invertebrates? A case study of larval dispersal between
747 the Bay of Biscay and the English Channel (North-East Atlantic). *Progress In*
748 *Oceanography* 87, 18–36.
- 749 Barillé, L., Bris, A.L., Gouletquer, P., Thomas, Y., Glize, P., Kane, F., Falconer, L.,
750 Guillotreau, P., Trouillet, B., Palmer, S., Gernez, P., 2020. Biological, socio-
751 economic, and administrative opportunities and challenges to moving aquaculture

- 752 offshore for small French oyster-farming companies. *Aquaculture* 735045.
753 <https://doi.org/10.1016/j.aquaculture.2020.735045>
- 754 Carson, H.S., López-Duarte, P.C., Rasmussen, L., Wang, D., Levin, L.A., 2010. Reproductive
755 Timing Alters Population Connectivity in Marine Metapopulations. *Current Biology*
756 20, 1926–1931. <https://doi.org/10.1016/j.cub.2010.09.057>
- 757 Choi, F., Gouhier, T., Lima, F., Rilov, G., Seabra, R., Helmuth, B., 2019. Mapping
758 physiology: biophysical mechanisms define scales of climate change impacts. *Conserv*
759 *Physiol* 7. <https://doi.org/10.1093/conphys/coz028>
- 760 Coscia, I., Robins, P.E., Porter, J.S., Malham, S.K., Ironside, J.E., 2013. Modelled larval
761 dispersal and measured gene flow: seascape genetics of the common cockle
762 *Cerastoderma edule* in the southern Irish Sea. *Conserv Genet* 14, 451–466.
763 <https://doi.org/10.1007/s10592-012-0404-4>
- 764 Davies, K.T.A., Gentleman, W.C., DiBacco, C., Johnson, C.L., 2014. Semi-annual spawning
765 in marine scallops strengthens larval recruitment and connectivity on Georges Bank: a
766 model study. *Marine Ecology Progress Series* 516, 209–227.
767 <https://doi.org/10.3354/meps10975>
- 768 DeAngelis, D.L., Yurek, S., 2017. Spatially Explicit Modeling in Ecology: A Review.
769 *Ecosystems* 20, 284–300. <https://doi.org/10.1007/s10021-016-0066-z>
- 770 Dormann, C.F., Schymanski, S.J., Cabral, J., Chuine, I., Graham, C., Hartig, F., Kearney, M.,
771 Morin, X., Römermann, C., Schröder, B., Singer, A., 2012. Correlation and process in
772 species distribution models: bridging a dichotomy. *Journal of Biogeography* 39, 2119–
773 2131. <https://doi.org/10.1111/j.1365-2699.2011.02659.x>
- 774 Dye, S., Hughes, S.L., Tinker, J., Berry, D.I., Holliday, N.P., Kent, E.C., Kennington, K.,
775 Inall, M., Smythe, T., Nolan, G., Lyons, K., Andres, O., Beszczynska-Möller, A.,
776 2013. Impacts of climate change on temperature (air and sea), in: Buckley, P.J.,
777 Baxter, J.M., Wallace, C.J. (Eds.), *Marine Climate Change Impacts Partnership*
778 *Science Review 2013*. MCCIP Secretariat.
- 779 Fearman, J., Moltschaniwskyj, N.A., 2010. Warmer temperatures reduce rates of
780 gametogenesis in temperate mussels, *Mytilus galloprovincialis*. *Aquaculture* 305, 20–
781 25. <https://doi.org/10.1016/j.aquaculture.2010.04.003>
- 782 Fly, E.K., Hilbish, T.J., Wetthey, D.S., Rognstad, R.L., 2015. Physiology and Biogeography:
783 The Response of European Mussels (*Mytilus* spp.) to Climate Change. *American*
784 *Malacological Bulletin* 33, 136–149. <https://doi.org/10.4003/006.033.0111>
- 785 Gilg, M.R., Howard, R., Turner, R., Middlebrook, M., Abdunour, M., Lukaj, E., Sheng, Y.P.,
786 Liu, T., Tutak, B., 2014. Estimating the dispersal capacity of the introduced green
787 mussel, *Perna viridis* (Linnaeus, 1758), from field collections and oceanographic
788 modeling. *Journal of Experimental Marine Biology and Ecology* 461, 233–242.
789 <https://doi.org/10.1016/j.jembe.2014.08.004>
- 790 Gilg, M.R., Kirby, S.E., Sullivan, R., Knapp, L.W., Hilbish, T.J., 2007. Dispersal vs.
791 retention: correspondence of species-specific reproductive cycles and settlement
792 periods in a blue mussel hybrid zone. *Marine Ecology Progress Series* 351, 151–161.
793 <https://doi.org/10.3354/meps07145>
- 794 Gohin, F., Druon, J.N., Lampert, L., 2002. A five channel chlorophyll concentration
795 algorithm applied to SeaWiFS data processed by SeaDAS in coastal waters. *Int. J.*
796 *Remote Sens.* 23, 1639–1661. <https://doi.org/10.1080/01431160110071879>

- 797 Gomes, I., Peteiro, L., Bueno-Pardo, J., Albuquerque, R., Pérez-Jorge, S., Oliveira, E.R.,
798 Alves, F.L., Queiroga, H., 2018. What's a picture really worth? On the use of drone
799 aerial imagery to estimate intertidal rocky shore mussel demographic parameters.
800 *Estuarine, Coastal and Shelf Science* 213, 185–198.
801 <https://doi.org/10.1016/j.ecss.2018.08.020>
- 802 Grimm, V., Berger, U., Bastiansen, F., Eliassen, S., Ginot, V., Giske, J., Goss-Custard, J.,
803 Grand, T., Heinz, S.K., Huse, G., Huth, A., Jepsen, J.U., Jørgensen, C., Mooij, W.M.,
804 Müller, B., Pe'er, G., Piou, C., Railsback, S.F., Robbins, A.M., Robbins, M.M.,
805 Rossmann, E., Rüger, N., Strand, E., Souissi, S., Stillman, R.A., Vabø, R., Visser,
806 U., DeAngelis, D.L., 2006. A standard protocol for describing individual-based and
807 agent-based models. *Ecological Modelling* 198, 115–126.
808 <https://doi.org/10.1016/j.ecolmodel.2006.04.023>
- 809 Grimm, V., Berger, U., DeAngelis, D.L., Polhill, J.G., Giske, J., Railsback, S.F., 2010. The
810 ODD protocol: A review and first update. *Ecological Modelling* 221, 2760–2768.
811 <https://doi.org/10.1016/j.ecolmodel.2010.08.019>
- 812 Guizien, K., Belharet, M., Marsaleix, P., Guarini, J.M., 2012. Using larval dispersal
813 simulations for marine protected area design: Application to the Gulf of Lions
814 (northwest Mediterranean). *Limnology and Oceanography* 57, 1099–1112.
815 <https://doi.org/10.4319/lo.2012.57.4.1099>
- 816 Guizien, K., Belharet, M., Moritz, C., Guarini, J.M., 2014. Vulnerability of marine benthic
817 metapopulations: implications of spatially structured connectivity for conservation
818 practice in the Gulf of Lions (NW Mediterranean Sea). *Diversity Distrib.* 20, 1392–
819 1402. <https://doi.org/10.1111/ddi.12254>
- 820 Haase, A.T., Eggleston, D.B., Luettich, R.A., Weaver, R.J., Puckett, B.J., 2012. Estuarine
821 circulation and predicted oyster larval dispersal among a network of reserves.
822 *Estuarine, Coastal and Shelf Science* 101, 33–43.
823 <https://doi.org/10.1016/j.ecss.2012.02.011>
- 824 Hawkins, S.J., Moore, P.J., Burrows, M.T., Poloczanska, E., Mieszkowska, N., Herbert,
825 R.J.H., Jenkins, S.R., Thompson, R.C., Genner, M.J., Southward, A.J., 2008. Complex
826 interactions in a rapidly changing world: responses of rocky shore communities to
827 recent climate change. *Climate Research* 37, 123–133.
828 <https://doi.org/10.3354/cr00768>
- 829 Hawkins, S.J., Sugden HE, Mieszkowska N, Moore PJ, Poloczanska E, Leaper R, Herbert
830 RJH, Genner MJ, Moschella PS, Thompson RC, Jenkins SR, Southward AJ, Burrows
831 MT, 2009. Consequences of climate-driven biodiversity changes for ecosystem
832 functioning of North European rocky shores. *Mar Ecol Prog Ser* 396, 245–259.
- 833 Helmuth, B., Harley, C.D.G., Halpin, P.M., O'Donnell, M., Hofmann, G.E., Blanchette, C.A.,
834 2002. Climate Change and Latitudinal Patterns of Intertidal Thermal Stress. *Science*
835 298, 1015–1017.
- 836 Hilbish, T.J., Lima, F.P., Brannock, P.M., Fly, E.K., Rognstad, R.L., Wetthey, D.S., 2012.
837 Change and stasis in marine hybrid zones in response to climate warming. *Journal of*
838 *Biogeography* 39, 676–687. <https://doi.org/10.1111/j.1365-2699.2011.02633.x>
- 839 Hubbard, A.B., Reidenbach, M.A., 2015. Effects of larval swimming behavior on the
840 dispersal and settlement of the eastern oyster *Crassostrea virginica*. *Marine Ecology*
841 *Progress Series* 535, 161–176. <https://doi.org/10.3354/meps11373>

- 842 Hughes, T.P., Baird, A.H., Dinsdale, E.A., Moltschaniwskyj, N.A., Pratchett, M.S.,
843 Tanner, J.E., Willis, B.L., 2000. Supply-side ecology works both ways: the link
844 between benthic adults, fecundity, and larval recruits. *Ecology* 81, 2241–2249.
- 845 Jolly, M.T., Jollivet, D., Gentil, F., Thiebaut, E., Viard, F., 2004. Sharp genetic break between
846 Atlantic and English Channel populations of the polychaete *Pectinaria koreni*, along
847 the North coast of France. *Heredity* 94, 23–32.
- 848 Jones, M.C., Cheung, W.W.L., 2015. Multi-model ensemble projections of climate change
849 effects on global marine biodiversity. *ICES Journal of Marine Science* 72, 741–752.
850 <https://doi.org/10.1093/icesjms/fsu172>
- 851 Jones, S.J., Lima, F.P., Wethey, D.S., 2010. Rising environmental temperatures and
852 biogeography: poleward range contraction of the blue mussel, *Mytilus edulis* L., in the
853 western Atlantic. *Journal of Biogeography* 37, 2243–2259.
854 <https://doi.org/10.1111/j.1365-2699.2010.02386.x>
- 855 Kearney, M., 2006. Habitat, environment and niche: what are we modelling? *Oikos* 115, 186–
856 191. <https://doi.org/10.1111/j.2006.0030-1299.14908.x>
- 857 Kearney, M., Simpson, S.J., Raubenheimer, D., Helmuth, B., 2010. Modelling the ecological
858 niche from functional traits. *Philosophical Transactions of the Royal Society B:*
859 *Biological Sciences* 365, 3469–3483.
- 860 Kearney, M.R., Gillingham, P.K., Bramer, I., Duffy, J.P., Maclean, I.M.D., 2020. A method
861 for computing hourly, historical, terrain-corrected microclimate anywhere on earth.
862 *Methods in Ecology and Evolution* 11, 38–43. [https://doi.org/10.1111/2041-](https://doi.org/10.1111/2041-210X.13330)
863 [210X.13330](https://doi.org/10.1111/2041-210X.13330)
- 864 Kim, C.-K., Park, K., Powers, S.P., 2013. Establishing Restoration Strategy of Eastern Oyster
865 via a Coupled Biophysical Transport Model. *Restoration Ecology* 21, 353–362.
866 <https://doi.org/10.1111/j.1526-100X.2012.00897.x>
- 867 Kooijman, S.A.L.M., 2010. *Dynamic Energy Budget Theory for Metabolic Organisation*.
868 Cambridge University Press, Cambridge.
- 869 Kooijman, S.A.L.M., 2006. Pseudo-faeces production in bivalves. *Journal of Sea Research*
870 56, 103–106.
- 871 Lal, M.M., Southgate, P.C., Jerry, D.R., Bosserelle, C., Zenger, K.R., 2016. A Parallel
872 Population Genomic and Hydrodynamic Approach to Fishery Management of Highly-
873 Dispersive Marine Invertebrates: The Case of the Fijian Black-Lip Pearl Oyster
874 *Pinctada margaritifera*. *PLoS ONE* 11, e0161390.
875 <https://doi.org/10.1371/journal.pone.0161390>
- 876 Laugen, A.T., Hollander, J., Obst, M., Strand, Å., 2015. 10. The Pacific Oyster (*Crassostrea*
877 *gigas*) Invasion in Scandinavian Coastal Waters: Impact on Local Ecosystem Services,
878 in: Canning-Clode, J. (Ed.), *Biological Invasions in Changing Ecosystems*. De Gruyter
879 Open, Warsaw, Poland. <https://doi.org/10.1515/9783110438666-015>
- 880 Lazure, P., Dumas, F., 2008. An external–internal mode coupling for a 3D hydrodynamical
881 model for applications at regional scale (MARS). *Advances in Water Resources* 31,
882 233–250.
- 883 Le Goff, C., Lavaud, R., Cugier, P., Jean, F., Flye-Sainte-Marie, J., Foucher, E., Desroy, N.,
884 Fifas, S., Foveau, A., 2017. A coupled biophysical model for the distribution of the

- 885 great scallop *Pecten maximus* in the English Channel. *Journal of Marine Systems*
886 167, 55–67. <https://doi.org/10.1016/j.jmarsys.2016.10.013>
- 887 Lett, C., Ayata, S.-D., Huret, M., Irisson, J.-O., 2010. Biophysical modelling to investigate
888 the effects of climate change on marine population dispersal and connectivity.
889 *Progress in Oceanography* 87, 106–113. <https://doi.org/10.1016/j.pocean.2010.09.005>
- 890 L'Hévéder, B., Speich, S., Ragueneau, O., Gohin, F., Bryère, P., 2017. Observed and
891 projected sea surface temperature seasonal changes in the Western English Channel
892 from satellite data and CMIP5 multi-model ensemble. *International Journal of*
893 *Climatology* 37, 2831–2849. <https://doi.org/10.1002/joc.4882>
- 894 Lowen, J.B., McKindsey, C.W., Therriault, T.W., DiBacco, C., 2016. Effects of spatial
895 resolution on predicting the distribution of aquatic invasive species in nearshore
896 marine environments. *Marine Ecology Progress Series* 556, 17–30.
897 <https://doi.org/10.3354/meps11765>
- 898 Lubet, P., 1959. Recherches sur le cycle sexuel et l'émission des gamètes chez les Mytilidés
899 et les Pectinidés (Mollusques bivalves). *Revue des Travaux de l'Institut des Pêches*
900 *Maritimes* 23, 397–547.
- 901 Malishev, M., Bull, C.M., Kearney, M.R., 2018. An individual-based model of ectotherm
902 movement integrating metabolic and microclimatic constraints. *Methods in Ecology*
903 *and Evolution* 9, 472–489. <https://doi.org/10.1111/2041-210X.12909>
- 904 Martin, B.T., Zimmer, E.I., Grimm, V., Jager, T., 2012. Dynamic Energy Budget theory
905 meets individual-based modelling: a generic and accessible implementation. *Methods*
906 *in Ecology and Evolution* 3, 445–449. <https://doi.org/10.1111/j.2041-210X.2011.00168.x>
- 908 Martin, M., Dash, P., Ignatov, A., Banzon, V., Beggs, H., Brasnett, B., Cayula, J.-F.,
909 Cummings, J., Donlon, C., Gentemann, C., Grumbine, R., Ishizaki, S., Maturi, E.,
910 Reynolds, R.W., Roberts-Jones, J., 2012. Group for High Resolution Sea Surface
911 temperature (GHRSSST) analysis fields inter-comparisons. Part 1: A GHRSSST multi-
912 product ensemble (GMPE). *Deep-Sea Res. Pt. II* 77–80, 21–30.
913 <https://doi.org/10.1016/j.dsr2.2012.04.013>
- 914 McQuaid, C.D., Phillips, T.E., 2000. Limited wind-driven dispersal of intertidal mussel
915 larvae: in situ evidence from the plankton and the spread of the invasive species
916 *Mytilus galloprovincialis* in South Africa. *Marine Ecology Progress Series* 201, 211–
917 220. <https://doi.org/10.3354/meps201211>
- 918 Ménesguen, A., Hachet, A., Grégoris, T., 2018. Modelling benthic invasion by the colonial
919 gastropod *Crepidula fornicata* and its competition with the bivalve *Pecten maximus*. 2.
920 Coupling the 0D model of colony-forming species to a connectivity matrix for a
921 realistic distributed simulation of benthic invasion. *Ecological Modelling* 375, 30–44.
922 <https://doi.org/10.1016/j.ecolmodel.2018.02.015>
- 923 Montalto, V., Helmuth, B., Ruti, P.M., Dell'Aquila, A., Rinaldi, A., Sarà, G., 2016. A
924 mechanistic approach reveals non linear effects of climate warming on mussels
925 throughout the Mediterranean sea. *Climatic Change* 139, 293–306.
926 <https://doi.org/10.1007/s10584-016-1780-4>
- 927 Nicolle, A., Dumas, F., Foveau, A., Foucher, E., Thiébaud, E., 2013. Modelling larval
928 dispersal of the king scallop (*Pecten maximus*) in the English Channel: examples from

- 929 the bay of Saint-Brieuc and the bay of Seine. *Ocean Dynamics* 63, 661–678.
930 <https://doi.org/10.1007/s10236-013-0617-1>
- 931 Nicolle, A., Moitié, R., Ogor, J., Dumas, F., Foveau, A., Foucher, E., Thiébaud, E., 2017.
932 Modelling larval dispersal of *Pecten maximus* in the English Channel: a tool for the
933 spatial management of the stocks. *ICES J Mar Sci* 74, 1812–1825.
934 <https://doi.org/10.1093/icesjms/fsw207>
- 935 North, E.W., King, D.M., Xu, J., Hood, R.R., Newell, R.I.E., Paynter, K., Kellogg, M.L.,
936 Liddel, M.K., Boesch, D.F., 2010. Linking optimization and ecological models in a
937 decision support tool for oyster restoration and management. *Ecological Applications*
938 20, 851–866. <https://doi.org/10.1890/08-1733.1>
- 939 North, E.W., Schlag, Z., Hood, R.R., Li, M., Zhong, L., Gross, T., Kennedy, V.S., 2008.
940 Vertical swimming behavior influences the dispersal of simulated oyster larvae in a
941 coupled particle-tracking and hydrodynamic model of Chesapeake Bay. *Marine*
942 *Ecology Progress Series* 359, 99–115.
- 943 Opaluch, J.J., Anderson, J.L., Schnier, K., 2009. A Risk-Based Approach to Managing the
944 Intentional Introduction of Non-Native Species 23.
- 945 Puckett, B.J., Eggleston, D.B., 2016. Metapopulation dynamics guide marine reserve design:
946 importance of connectivity, demographics, and stock enhancement. *Ecosphere* 7,
947 e01322. <https://doi.org/10.1002/ecs2.1322>
- 948 R Development Core Team, 2012. R: A language and environment for statistical computing.
949 R Foundation for Statistical Computing, Vienna, Austria. <http://www.R-project.org/>.
- 950 Roughgarden, J., Iwasa, Y., Baxter, C., 1985. Demographic Theory for an Open Marine
951 Population with Space-Limited Recruitment. *Ecology* 66, 54–67.
952 <https://doi.org/10.2307/1941306>
- 953 Saraiva, S., Van Der Meer, J., Kooijman, S.A.L.M., Witbaard, R., Philippart, C.J.M., Hippler,
954 D., Parker, R., 2012. Validation of a Dynamic Energy Budget (DEB) model for the
955 blue mussel *Mytilus edulis*. *Mar Ecol Prog Ser* 463, 141–158.
- 956 Saulquin, B., Gohin, F., 2010. Mean seasonal cycle and evolution of the sea surface
957 temperature from satellite and in situ data in the English Channel for the period 1986–
958 2006. *International Journal of Remote Sensing* 31, 4069–4093.
959 <https://doi.org/10.1080/01431160903199155>
- 960 Saulquin, B., Gohin, F., Garrello, R., 2011. Regional Objective Analysis for Merging High-
961 Resolution MERIS, MODIS/Aqua, and SeaWiFS Chlorophyll-a Data From 1998 to
962 2008 on the European Atlantic Shelf. *IEEE Trans. Geosci. Remote Sens.* 49, 143–154.
963 <https://doi.org/10.1109/TGRS.2010.2052813>
- 964 Scheffer, M., Baveco, J.M., DeAngelis, D.L., Rose, K.A., van Nes, E.H., 1995. Super-
965 individuals a simple solution for modelling large populations on an individual basis.
966 *Ecological Modelling* 80, 161–170. [https://doi.org/10.1016/0304-3800\(94\)00055-M](https://doi.org/10.1016/0304-3800(94)00055-M)
- 967 Shpigel, M., Barber, B.J., Mann, R., 1992. Effects of elevated temperature on growth,
968 gametogenesis, physiology, and biochemical composition in diploid and triploid Pacific
969 oysters: *Crassostrea gigas* Thunberg. *Journal of Experimental Marine Biology and*
970 *Ecology* 161, 15–25.
- 971 Southward, A.J., Langmead, O., Hardman-Mountford, N.J., Aiken, J., Boalch, G.T., Dando,
972 P.R., Genner, M.J., Joint, I., Kendall, M.A., Halliday, N.C., Harris, R.P., Leaper, R.,

- 973 Mieszkowska, N., Pingree, R.D., Richardson, A.J., Sims, D.W., Smith, T.,
974 Walne, A.W., Hawkins, S.J., 2004. Long-Term Oceanographic and Ecological
975 Research in the Western English Channel, in: *Advances in Marine Biology*. Academic
976 Press, pp. 1–105. [https://doi.org/10.1016/S0065-2881\(04\)47001-1](https://doi.org/10.1016/S0065-2881(04)47001-1)
- 977 Sprung, M., 1984. Physiological energetics of mussel larvae (*Mytilus edulis*). I. Shell growth
978 and biomass. *Marine Ecology Progress Series* 17, 283–293.
- 979 Thomas, Y., Bacher, C., 2018. Assessing the sensitivity of bivalve populations to global
980 warming using an individual-based modelling approach. *Glob Change Biol* 24, 4581–
981 4597. <https://doi.org/10.1111/gcb.14402>
- 982 Thomas, Y., Pouvreau, S., Alunno-Bruscia, M., Barillé, L., Gohin, F., Bryère, P., Gernez, P.,
983 2016. Global change and climate-driven invasion of the Pacific oyster (*Crassostrea*
984 *gigas*) along European coasts: a bioenergetics modelling approach. *J. Biogeogr.* 43,
985 568–579. <https://doi.org/10.1111/jbi.12665>
- 986 van Vuuren, D.P., Edmonds, J., Kainuma, M., Riahi, K., Thomson, A., Hibbard, K., Hurtt,
987 G.C., Kram, T., Krey, V., Lamarque, J.-F., Masui, T., Meinshausen, M., Nakicenovic,
988 N., Smith, S.J., Rose, S.K., 2011. The representative concentration pathways: an
989 overview. *Climatic Change* 109, 5. <https://doi.org/10.1007/s10584-011-0148-z>
- 990 Watson, J.R., Mitarai, S., Siegel, D.A., Caselle, J.E., Dong, C., McWilliams, J.C., 2010.
991 Realized and potential larval connectivity in the Southern California Bight. *Marine*
992 *Ecology Progress Series* 401, 31–48. <https://doi.org/10.3354/meps08376>
- 993 Wethey, D.S., Woodin, S.A., Hilbish, T.J., Jones, S.J., Lima, F.P., Brannock, P.M., 2011.
994 Response of intertidal populations to climate: Effects of extreme events versus long
995 term change. *Journal of Experimental Marine Biology and Ecology* 400, 132–144.
996 <https://doi.org/10.1016/j.jembe.2011.02.008>
- 997 Yasuoka, N., Yusa, Y., 2016. Effects of size and gregariousness on individual sex in a natural
998 population of the Pacific oyster *Crassostrea gigas*. *Journal of Molluscan Studies* 82,
999 485–491. <https://doi.org/10.1093/mollus/eyw020>
- 1000 Yusa, Y., Breton, S., Hoeh, W.R., 2013. Population Genetics of Sex Determination in *Mytilus*
1001 *Mussels: Reanalyses and a Model*. *Journal of Heredity* 104, 380–385.
1002 <https://doi.org/10.1093/jhered/est014>
- 1003 Zhang, X., Haidvogel, D., Munroe, D., Powell, E.N., Klinck, J., Mann, R., Castruccio, F.S.,
1004 2015. Modeling larval connectivity of the Atlantic surfclams within the Middle
1005 Atlantic Bight: Model development, larval dispersal and metapopulation connectivity.
1006 *Estuarine, Coastal and Shelf Science* 153, 38–53.
1007 <https://doi.org/10.1016/j.ecss.2014.11.033>
- 1008
- 1009